

Biomass-derived Activated Carbon for Rechargeable Lithium-Sulfur Batteries

Min Liu,^a Yong Chen,^{a,*} Ke Chen,^a Na Zhang,^a Xiaoqin Zhao,^a Fenghui Zhao,^a Zhifeng Dou,^a Xiangming He,^b and Li Wang^b

High-surface-area activated carbon (HSAAC) was synthesized by carbonizing coconut shells and subsequently activating the material with KOH. The as-prepared HSAAC had a mostly microporous structure (with small mesoporous inclusions) and exhibited a high specific surface area of 2258.7 m²g⁻¹ and an average pore size of 2.246 nm. Sulfur was then loaded into the activated carbon (AC), and this S/HSAAC (62 wt%) was used as a cathode for Li-S batteries. These batteries delivered an initial discharge capacity of 1233 mAhg⁻¹ at a current density of 200 mA g⁻¹. Due to the strong absorption force of the micropores and a high pore volume, the cells retained 929 mAhg⁻¹ with 80% capacity retention of the initial discharge after 100 cycles. Considering its low cost and ability to be produced at a large-scale, biomass-derived HSAAC is a promising electrode material that may advance high-energy rechargeable lithium-sulfur batteries toward use in practical applications.

Keywords: Biomass; Activated carbon; Li-S battery

Contact information: a: Laboratory of Tropic Biological Resources of Ministry of Education, Key Laboratory of Ministry of Education for Advanced Materials in Tropical Island Resources, Hainan Provincial Key Laboratory of Research on Utilization of Si-Zr-Ti Resources, Hainan University, Haikou, Hainan 570228, PR China; b: Institute of Nuclear & New Energy Technology, Tsinghua University, Beijing 100084, PR China; * Corresponding author: ychen2002@163.com

INTRODUCTION

To overcome the limited energy density of the present lithium-ion batteries, high energy density rechargeable batteries have been gaining more attention in recent years (Tarascon and Amand 2001; Goodenough and Kim 2010; Chen *et al.* 2011; Scrosati *et al.* 2011; Kicinski *et al.* 2014). Among them, the Li-S battery is an appealing candidate due to its high theoretical specific capacity of 1675 mAhg⁻¹ and energy density of 2600 Whkg⁻¹, which is five times higher than that of a presently commercialized LiCoO₂ cathode. In addition, elemental sulfur has the advantages of low cost, non-toxicity, and natural abundance (Thackeray *et al.* 2012; Chung and Manthiram 2014). However, lithium-sulfur batteries suffer from capacity fading during charge/discharge cycling, which impedes their commercialization (Shim *et al.* 2002; Yang *et al.* 2013; Song *et al.* 2013). This capacity fade is due to three main factors: 1) sulfur and the discharge product Li₂S are both insulators; 2) the reduced product (Li₂S) deposits on the reaction interface, which blocks the inrush of electrolyte and reduces S utilization; 3) polysulfides (Li₂S_x, 4 < X ≤ 8) dissolve in the electrolyte causing a subsequent shuttle phenomenon (Peled *et al.* 1998; Kolosnitsyn and Karaseva 2008; Kang and Ceder 2009; Wang *et al.* 2010; Elazari *et al.* 2011; Lee *et al.* 2012; Diao *et al.* 2013).

To solve these problems, more attention has been given to the tunable design of the host structure and the preparation of the electrode materials (Manthiram *et al.* 2008;

Liang *et al.* 2009; Ji *et al.* 2009; Jayaprakash *et al.* 2011; Guo *et al.* 2011; Cao *et al.* 2011; Wang *et al.* 2011; Sun *et al.* 2012; Park *et al.* 2013). One of the most effective methods has been embedding S into conductive hosts such as microporous carbon (Zheng *et al.* 2006; Zhang *et al.* 2013), mesoporous carbon (Wang *et al.* 2008; Li *et al.* 2011; Zhang *et al.* 2014), carbon fibers (Zheng *et al.* 2011; Ji *et al.* 2011; Deng *et al.* 2013), amorphous carbon nanotubes (Yin *et al.* 2011; Dorfler *et al.* 2012), and graphene (Yan *et al.* 2009; Wang *et al.* 2011; Zhou *et al.* 2014). In these studies, the carbon-sulfur composite used in lithium-sulfur batteries exhibited high active mass utilization and excellent cycle stability; it also benefited from good electrical conductivity, large pore volume, and high surface area of the carbon host (Wei *et al.* 2012). Unfortunately, most of these materials require complex synthesis procedures that restrict their feasibility for large scale applications.

To address this issue, we focused on the utilization of renewable biomass materials, which are produced in large amounts in tropical areas annually, and they have been used to produce AC (Jayaprakash *et al.* 2011; Cao *et al.* 2011; Li *et al.* 2011; Park *et al.* 2013) due to their excellent natural porous structure and low ash content. It is believed that AC will likely remain a major emphasis for commercial applications research due to its scalability, low cost, and more reliable production (Wei *et al.* 2013). In this work, our aim is to research the feasibility of mass production of inexpensive activated carbon electrode materials for Li-S batteries. If coconut-shell-based AC can be successfully used as an electrode material, the cost of Li-S batteries will be greatly reduced, thus facilitating widely adopted commercial application. Therefore, activated carbon with a mostly microporous structure (with a small mesoporous inclusions) and large surface area was produced by carbonizing coconut shells and subsequent activation. The large microporosity of the product allowed sulfur to be encapsulated, which ensured good electrical contact between sulfur and the conductive carbon framework (Zheng *et al.* 2006; Park *et al.* 2013; Zhang *et al.* 2013), which lead to high capacity and excellent cycle ability. The S/HSAAC composite was prepared by a simple melt-diffusion process, with the electrochemical performance of the cathode investigated in detail.

EXPERIMENTAL

Activation of Carbon Derived from Coconut Shells

Activated carbon was obtained by the thermal carbonization of coconut shells, a high volume waste product from Hainan (China). The typical preparation procedure was as follows: first, the coconut shells were smashed and dried at 120 °C for 12 h, followed by carbonization at 350 °C for 2 h under N₂ flow. Then a mixture of carbonized material and KOH with the weight ratio of 1:4 was ground and heated in a tube furnace at 300 °C for 30 min, then at 750 °C for 1 h under N₂ flow. The product was washed by distilled water until the pH= 7.0 and then dried.

Preparation and Characterization of Sulfur/Carbon Composites

S/HSAAC composites were prepared via a melt-diffusion method (Sun *et al.* 2012; Park *et al.* 2013). The as-prepared HSAAC was ground with sublimed sulfur (AR) with the weight ratio of 4:6 and sealed in a 25 mL Teflon-lined autoclave. This was followed by heating the mixture at 155 °C for 24 h; due to its low viscosity at this temperature, the molten sulfur easily diffused into the meso/micropores of the HSAAC. The sulfur content

in the composites was 60 wt% (Fig. 1), which was confirmed by a thermogravimetric analyzer (NETZSCH, STA449C) under an Ar atmosphere. The morphology and microstructure of the HSAAC and the S/HSAAC composite were detected with a scanning electron microscope (SEM, HITACHZS-4800), Brunauer Emmett Teller analysis (BET, JW-BK112) and X-ray diffraction (XRD, Bruker D8 Advance).

Electrochemical Measurements

The S/HSAAC composite was mixed with conductive carbon black and polytetrafluorethylene (PTFE) with a mass ratio of 8:1:1, using ethanol as a dispersant. The paste was then pressed into a film with a roller, which was cut into 10 mm diameter pieces and dried at 50 °C for 24 h in a vacuum. 2025 coin cells were assembled using the S/HSAAC composite as the cathodes and Li metal as the anodes in an Ar-filled glovebox. The electrolyte was LiTFSI (1 M, Sigma Aldrich) dissolved in a mixture of 1,2-dimethoxyethane (DME, Sigma Aldrich) and 1,3 dioxolane (DOL, Sigma Aldrich) (1:1, vol), with 0.25 M LiNO₃ as an additive. Cyclic voltammetry (CV) and electrochemical impedance spectroscopy (EIS) measurements were conducted on an electrochemical workstation CHI760E. CV tests were performed at a scan rate of 0.1 mVs⁻¹ in the voltage range of 1.5 to 3.2 V. EIS measurements were carried out at open-circuit potential in the frequency range between 0.1Hz and 10⁶ Hz with a perturbative amplitude of 5 mV. Galvanostatic charge/discharge tests were performed in the potential range of 1.7 to 2.8 V at 26 °C by using a LAND CT2001A battery-testing instrument.

RESULTS AND DISCUSSION

The sulfur content in the as-prepared S/HSAAC composites was measured by thermogravimetric analysis (TG) under an Ar atmosphere, and the results are shown in Fig. 1.

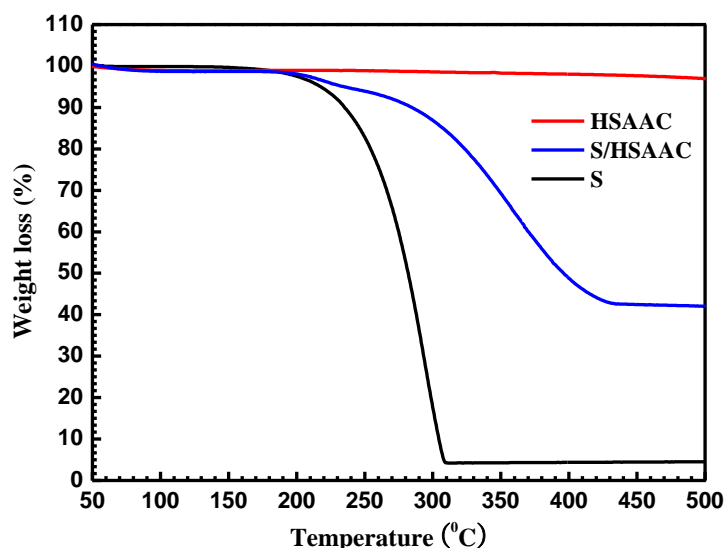


Fig. 1. TG curves of the as-prepared HSAAC, S/HSAAC composites, and pure sulfur recorded under an Ar atmosphere with a heating rate of 10 °C min⁻¹

While pure sulfur evaporates completely by 310 °C, the weight lost with increasing temperature S/HSAAC composites can be observed to occur much more slowly than that of pure sulfur until 420 °C; this is possibly due to the micropore adsorption force on the sulfur. From the TG curves, one can see that the sulfur content of the S/HSAAC composites was 62 wt%.

N₂ adsorption/desorption measurements were employed to investigate the porous structure of HSAAC as shown in Fig. 2(a). BET specific surface areas calculated from adsorption isotherms show that the specific surface area decreased dramatically from 2258.7 m²g⁻¹ for the HSAAC to 626.7 m²g⁻¹ after sulfur loading (Table 1). Simultaneously, the corresponding pore volumes decreased from 1.23 cm³g⁻¹ for the HSAAC to 0.34 cm³g⁻¹ for the composite. This shows that sulfur has been encapsulated into the pores of the host HSAAC matrix, resulting in the observed dramatic decrease in the surface area and pore volume.

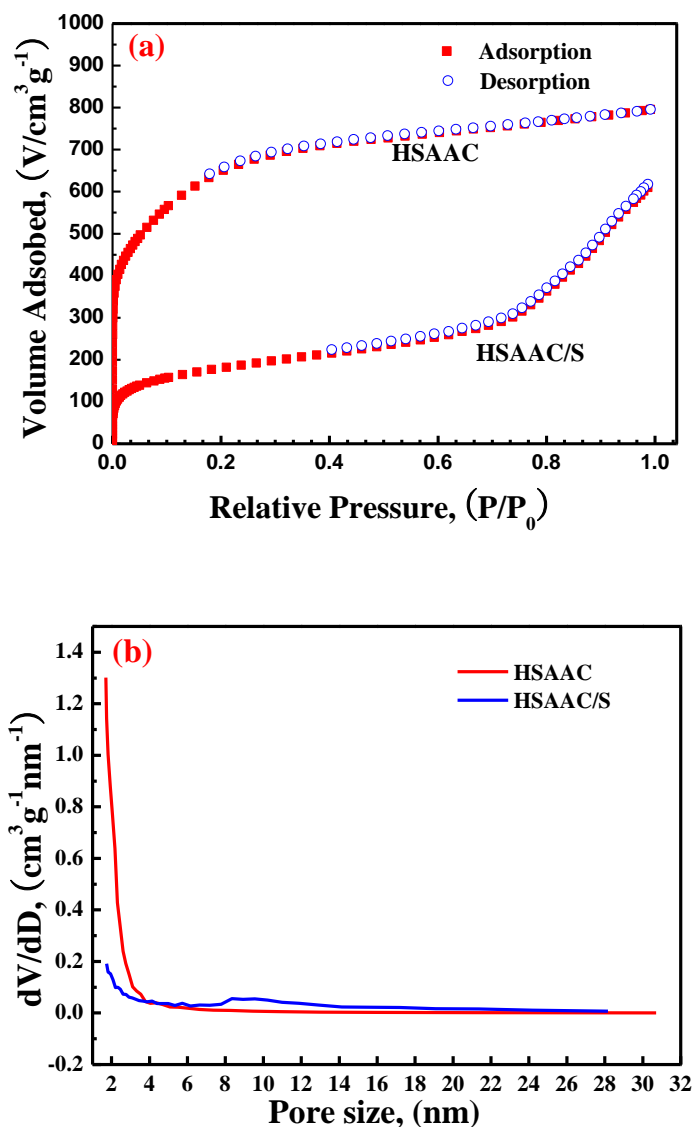


Fig. 2. (a) Nitrogen adsorption and desorption isotherms at 77 K for HSAAC before and after sulfur loading; (b) pore size distributions of HSAAC and S/HSAAC composites

The pore size distributions of the HSAAC and the S/HSAAC composites were calculated by using the Barrett-Joyner-Halenda (BJH) method (Kruk and Jaroniec 2002). As can be seen in Fig. 2(b), the HSAAC had a large amount of micropores with a diameter below 2 nm. Correspondingly, the micropores contributed to the large specific surface area of 2258.7 m²g⁻¹. The narrow abundant micropores of HSAAC could accommodate molten sulfur with either S₈ crown rings or linear-chain shapes due to their strong adsorption, allowing for a high dispersion of sulfur in the micropores (Zheng *et al.* 2006; Zhang *et al.* 2013). After loading 62 wt% sulfur into the HSAAC host, the curve at a pore diameter smaller than 2 nm declined and a small amount of mesoporous inclusion (~10 nm) emerged, which may have been due to new formations of the sulfur that was loaded into macroporous inclusions of HSAAC after melt-diffusion or to the activation process of carbonizing coconut shells (Wang *et al.* 2007; Li *et al.* 2011; Moreno *et al.* 2014; Zhang *et al.* 2014). These mesoscale pores could facilitate the movement of Li⁺ in the electrochemical process. The comparison between the pore size distributions of the HSAAC and the S/HSAAC composite revealed that most micropores (~2 nm) present in HSAAC were no longer present in S/HSAAC, and were filled with sulfur.

The surface areas and total pore volumes of the HSAAC and S/HSAAC composite estimated using the BET and BJH methods are summarized in Table 1.

Table 1. Physical Properties of the HSAAC and HSAAC/S Composite

	HSAAC	HSAAC/S
Pore size (nm)	2.246	6.095
Surface area (m ² /g)	2258.722	626.783
Pore volume (cm ³ /g)	1.230	0.343

The XRD patterns of the HSAAC, S/HSAAC composite, and sublimated sulfur are shown in Fig. 3.

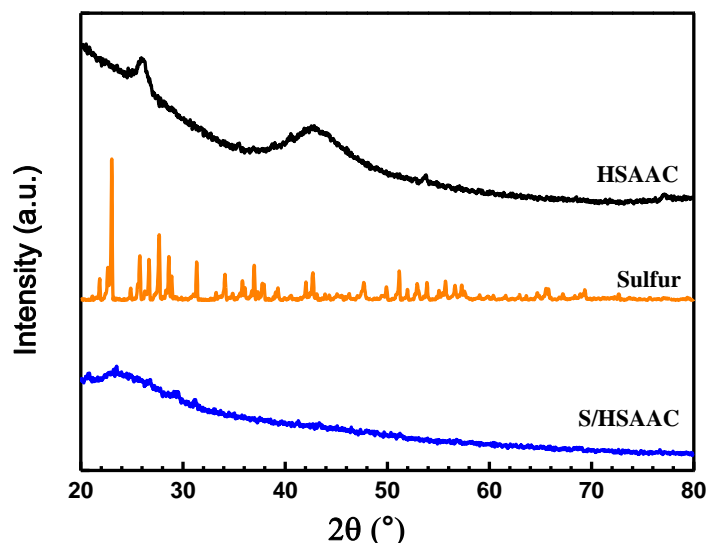


Fig. 3. XRD patterns of HSAAC, sublimated sulfur, and S/HSAAC composite

The characteristic peaks of sulfur and HSAAC were clearly observable, while no characteristic peak of sulfur was observed for the S/HSAAC composite; this indicated that the sulfur was in an amorphous form and was trapped in the micropores of the HSAAC.

Figure 4 shows SEM images of the HSAAC and S/HSAAC composite. It revealed a HSAAC structure with a spongy appearance (Fig. 4a). After sulfur loading (Fig. 4b), the surface of the HSAAC became rougher as the sulfur particles gathered and was more ambiguous. During the melt-diffusion process, the mixture of sulfur particles could melt and infiltrate the porous framework of the HSAAC due to the large pore volume and strong microporous adsorption capability of the carbon matrix. As a result, sulfur was uniformly diffused into the highly porous carbon.

To further verify the structure and composition of our S/HSAAC composite, energy dispersive spectroscopic (EDS) mapping/imaging (Fig. 5) of S/HSAAC was carried out. Clearly, carbon and sulfur elements were detected from a selected area of the S/HSAAC composite, confirming the presence of sulfur. In summary, from the BET and SEM results we concluded that sulfur is homogeneously distributed throughout the composite, and most of the sulfur was contained within the interior of the pore structure.

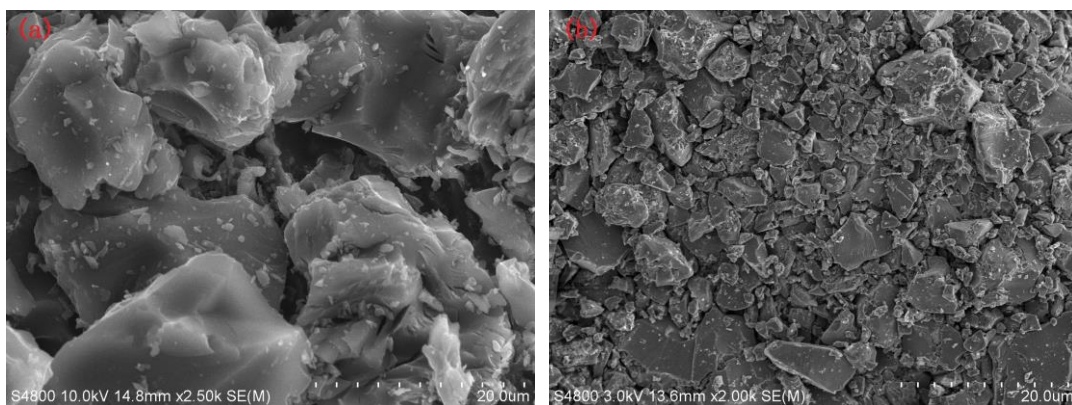


Fig. 4. SEM images of (a) the HSAAC and (b) S/HSAAC composite

A cyclic voltammogram of the S/HSAAC composite is given in Fig. 6(a). During the first cathodic scan, one can observe two reduction peaks at 2.02 V (vs. Li/Li+) and 2.28 V, which can be attributed to the two-step reduction of sulfur with metallic lithium (Kumaresan *et al.* 2008). The peak below 1.8 V indicated the transformation from S₂₋₄ (so-called “small molecule” sulfur) that was trapped in the micropores of HSAAC) to S²⁻ (Mikhaylik and Akridge 2004).

In the first anodic scan, only one sharp oxidation peak appeared at 2.38 V, which corresponds to the oxidation of Li₂S and Li₂S into polysulfides. In the following cycles, the cathodic peak potentials transferred to about 2.3 V and 2.06 V, which may be attributed to the polarization of the electrode in the first cycle. One can see that the CV waves all returned to the base line, meaning the formation of thin layer behavior, which supports the growth of reduced forms of Li_xS_y. In general, the cathodic and anodic peaks remained almost unchanged, confirming good reversibility and cycling performance after the initial electrochemical process.

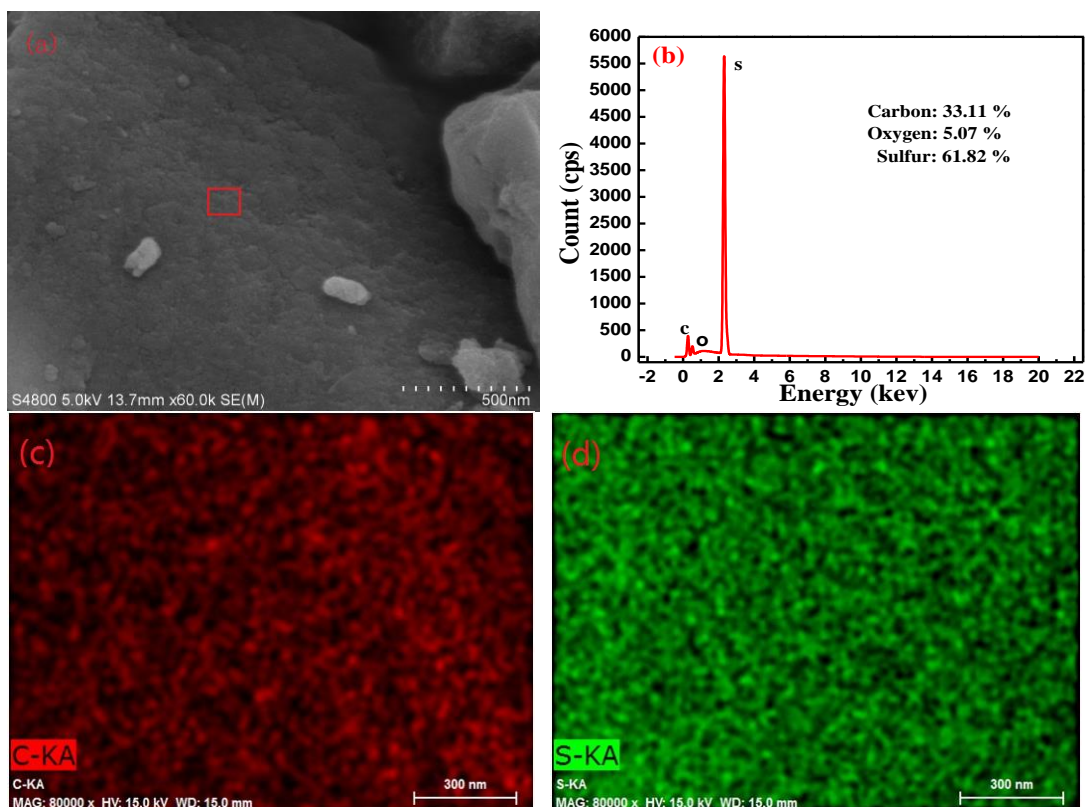


Fig. 5. EDS characterization of S/HSAAC composite: (a) SEM image of S/HSAAC composite; (b) EDS spectrum captured for the region shown in (a); (c) EDS sulfur and (d) carbon mapping of the region shown in (a).

Figure 6(b) shows the initial three charge/discharge curves of the S/HSAAC composite at a current density of 200 mA g^{-1} . The two discharge voltage plateaus at 2.3 and 2.1 V and the single charge voltage plateau at 2.38 V observed during the initial cycle for the S/HSAAC composite were in accordance with the CV measurements in Fig. 6(a). The first discharge capacity was 1233 mAh g^{-1} , on the basis of the weight of sulfur, with an initial coulombic efficiency of 99.5%. In subsequent cycles, a reversible capacity of around 1150 mAh g^{-1} was obtained, which was about 70% of the theoretical capacity of 1675 mAh g^{-1} . This differed greatly from the widely-reported low efficiency of lithium-sulfur battery at the first few cycles (Chen *et al.* 2011; Lee *et al.* 2012; Diao *et al.* 2013; Zhang *et al.* 2013). After the 50th and 100th cycles, there was still no obvious decline in capacity during cycling, revealing a high reversibility.

The cycling performance of the S/HSAAC composite is given in Fig. 7(a). The material showed excellent cycling durability. The capacity decrease in the first few cycles may be due to solubility of lithium polysulfides and the insulating reduction product Li_2S depositing on the cathode surface (Mikhaylik and Akridge 2004). The capacity then decreased slightly, while maintaining a coulombic efficiency of no less than 99.5 % in the subsequent cycles. After 100 cycles the discharge capacity still was 929 mAh g^{-1} . The high cycling stability of the S/HSAAC composite could be attributable to several factors. The highly dispersed sulfur in the pores of the HSAAC may have successfully buffered the volume effects of the charge/discharge process. Additionally, the large specific surface area originating from the micropores in the HSAAC may restrict the diffusion of the polysulfides during the cycling process (Ji *et al.* 2011; Zhang *et al.* 2013, 2014).

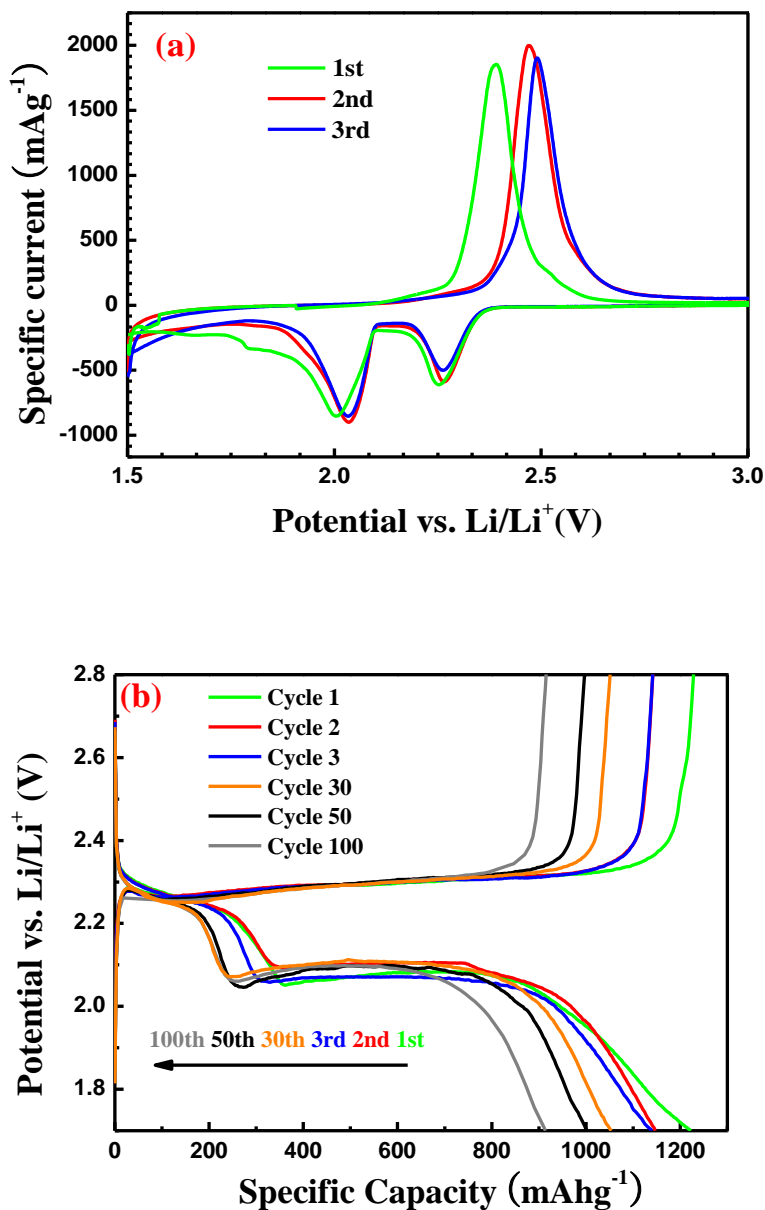


Fig. 6. (a) Cyclic voltammograms of the S/HSAAC composite at 0.1 mVs⁻¹; (b) charge/discharge profiles of a Li-S cell with a S/HSAAC composite cathode with a current density of 200 mA_hg⁻¹

The high-rate discharge capability and cycle performance of the S/HSAAC composite after 100 cycles were measured at various current densities, as shown in Fig. 7(b). The discharge capacity was relatively stable at various current densities. The high retention of capacity while increasing the current density from 200 mA_g⁻¹ to 800 mA_g⁻¹ should be noted; even at the high current density of 1600 mA_g⁻¹, a capacity of 768 mA_g⁻¹ could still be obtained. A reversible capacity of 436 mA_hg⁻¹ was still obtained at the high current density of 3200 mA_g⁻¹. After the current density was restored to 200 mA_g⁻¹, the capacity returned to as high as 874 mA_hg⁻¹ after 200 cycles, indicating an excellent reversibility.

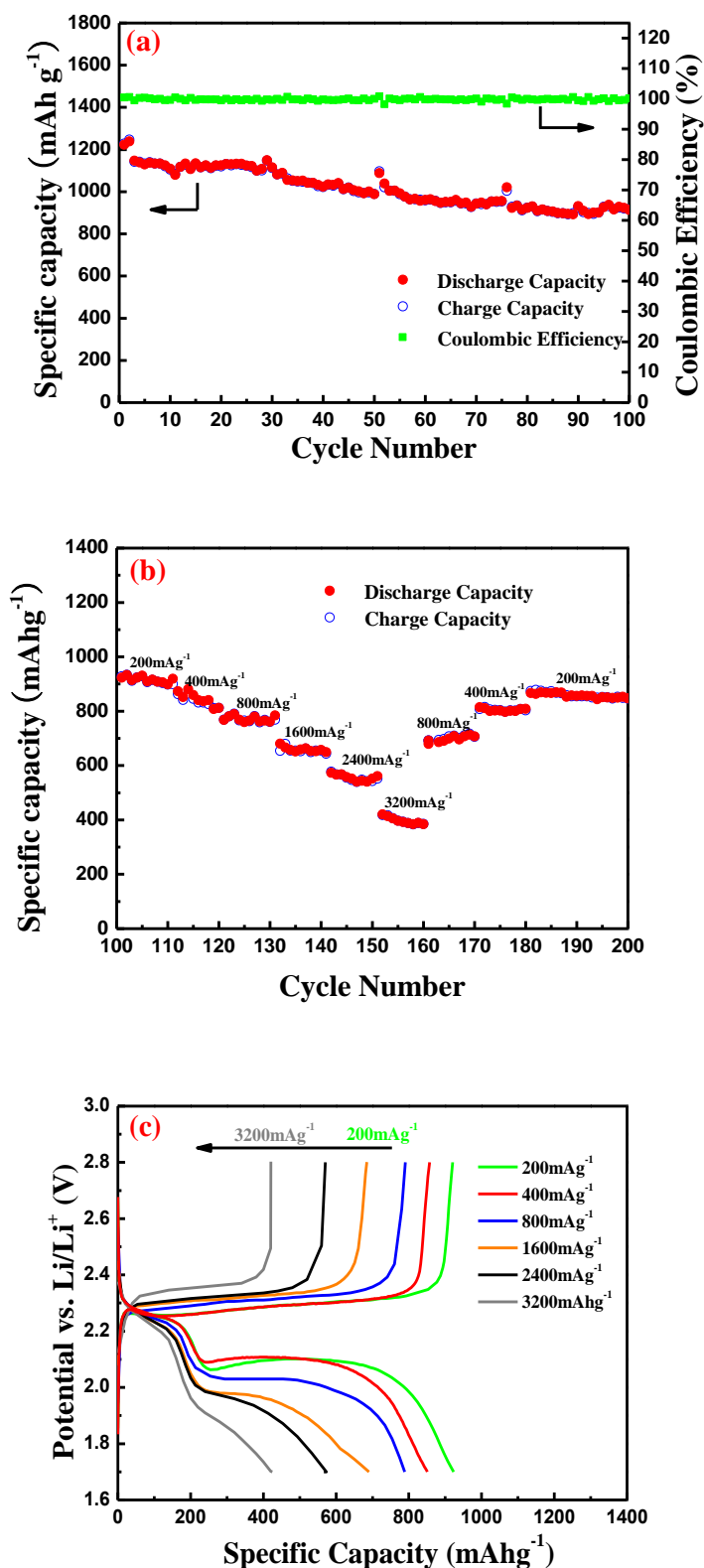


Fig. 7. (a) Cycling performance at the current density of 200 mA h⁻¹; (b) rate capabilities of the S/HSAAC composite after 100 cycles; (c) galvanostatic charge-discharge curves at different current densities after 100 cycles

The obvious polarization and distortion emerged with increasing current density, as shown in the charge-discharge curves Fig. 7(c), undoubtedly, the mostly microporous (with a few mesoporous inclusions) carbon structure played a major role in the electrochemical performance of S/HSAAC. The essential factor in the high performance of S/HSAAC was that its microporosity provided a large pore volume to the structure and functioned as a reservoir for trapping the polysulfides, thereby restraining the shuttle phenomenon (Mikhaylik and Akridge 2004; Zhang *et al.* 2013, 2014). The mesoporous system facilitated Li^+ movement and good capacity retention. This is much different from the mesoporous system, which gave rise to an outflow of sulfur with a weak adsorption capability problem; the microporous system, owing to poor infiltration of the electrolyte, hindered the movement of Li^+ (Li *et al.* 2011; Zhang *et al.* 2013; Moreno *et al.* 2014; Zhang *et al.* 2014). Because of its enhanced active material utilization, excellent conductivity, large surface area, narrow micropores with strong adsorption, and electrochemical cyclability, HSAAC is a promising cathode material for rechargeable Li-S batteries. Its high capacity and simple synthesis process give it great potential for mass production in future commercial applications.

Figure 8 presents the EIS analysis of the S/HSAAC composite cathode after the 1st, 20th, and 100th cycles. The plots of cells exhibited a depressed semicircle followed by an inclined line in the low frequency region. The semicircles correspond to the charge transfer resistance (R_{ct}) at the interface of cathode, and the inclined line in the low frequency region is the diffusion impedance of Li ions in the composite. It is obvious that the overall impedance increased dramatically with the number of discharge/charge cycles.

The electrolyte resistance (R_e) increased only slightly, which is related to the dissolved Li polysulfides in the electrolyte. The deposition of insulating Li_2S_2 and Li_2S at the interface on the cathode contributed to the increase of R_{ct} (Zhang *et al.* 2014; Zhou *et al.* 2014).

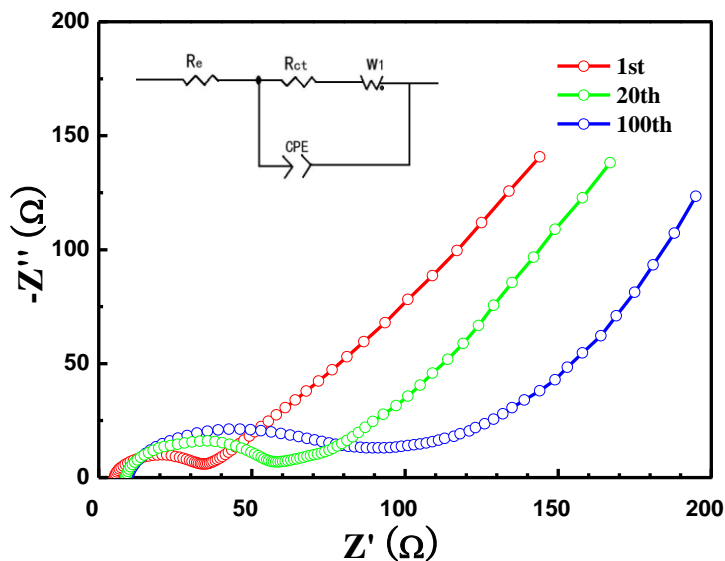


Fig. 8. Impedance plots for the S/HSAAC composite cathode after 1st, 20th, and 100th discharge cycles

CONCLUSIONS

High-surface-area carbon derived from coconut shells and activated by KOH was loaded with sulfur and used as a cathode for lithium/sulfur batteries. Due to the combination of the microporosity of the activated carbon trapping elemental S and Li polysulfides and the mesoporosity of the system facilitating the Li⁺ movement during cycling, the S/HSAAC composite exhibited a high initial discharge capacity of 1233 mAhg⁻¹ at the current density of 200 mAhg⁻¹ with a coulombic efficiency of 99.9% and a capacity retention of 929 mAhg⁻¹ after 100 cycles.

ACKNOWLEDGEMENTS

This work is supported by NSFC (51362009 and 51162006) and MOST (2013CB934000, 2013AA050903) of China.

REFERENCES CITED

- Cao, Y., Li, X., Aksay, I. A., Lemmon, J., Nie, Z., Yang, Z., and Liu, J. (2011). "Sandwich-type functionalized graphene sheet-sulfur nanocomposite for rechargeable lithium batteries," *Phys. Chem. Chem. Phys.* 13(3), 7660-7665. DOI:10.1039/c0cp02477e
- Chen, Y., Li, C., Wang, Y., Zhang, Q., Xu, C., Wei, B., and An, L. J. (2011). "Self-assembled carbon-silicon carbonitride nanocomposites: High-performance anode materials for lithium-ion batteries," *J. Mater. Chem.* 21(45), 18186-18190. DOI:10.1039/C1JM13733F
- Chung, S. H., and Manthiram, A. (2014). "Low-cost porous carbon current collector with high sulfur loading for lithium-sulfur batteries," *Electrochem. Commun.* 38(11), 91-95. DOI:10.1016/j.elecom.2013.11.008
- Deng, Z., Zhang, Z., Lai, Y., Liu, J., Liu, Y., and Li, J. (2013). "A sulfur-carbon composite for lithium/sulfur battery based on activated vapor-grown carbon fiber," *Solid State Ionics* 238(4), 44-49. DOI: 10.1016/j.ssi.2013.03.018
- Diao, Y., Xie, K., Xiong, S. Z., and Hong, X. B. (2013). "Shuttle phenomenon-the irreversible oxidation mechanism of sulfur active material in Li-S battery," *J. Power Sources* 235(1), 181-186. DOI: 10.1002/adma.201103274
- Dorfler, S., Hagen, M., Althues, H., Tubke, J., Kaskel, S., and Hoffmann, M. J. (2012). "High capacity vertical aligned carbon nanotube/sulfur composite cathodes for lithium-sulfur batteries," *Chem. Commun.* 48(34), 4097-4099. DOI: 10.1039/C2CC17925C
- Elazari, R., Salitra, G., Garsuch, A., Panchenko, A., and Aurbach, D. (2011). "Sulfur-impregnated activated carbon fiber cloth as a binder-free cathode for rechargeable Li-S batteries," *Adv. Mater.* 23(47), 5641-5644. DOI: 10.1002/adma.201103274
- Goodenough, J. B., and Kim, Y. (2010). "Challenges for rechargeable Li batteries," *Chem. Mater* 22(3), 587-603. DOI:10.1021/cm901452z
- Guo, J. C., Xu, Y. H., and Wang, C. S. (2011). "Sulfur-impregnated disordered carbon nanotubes cathode for lithium-sulfur batteries," *Nano Lett.* 11(10), 4288-4294. DOI: 10.1021/nl202297p

- Ji, X., Lee, K. T., and Nazar, L. (2009). "A highly ordered nanostructured carbon-sulfur cathode for lithium-sulphur batteries," *Nat. Mater.* 8(5), 500-506. Doi:10.1038/nmat2460
- Ji, L., Rao, M., Aloni, S., Wang, L., Cairns, E. J., and Zhang, Y. (2011). "Porous carbon nanofiber-sulfur composite electrodes for lithium/sulfur cells," *Energy Environ. Sci.* 4(12), 5053-5059. DOI: 10.1039/C1EE02256C
- Jayaprakash, N., Shen, J., Moganty, S. S., Corona, A., and Archer, L. A. (2011). "Porous hollow carbon@sulfur composites for high-power lithium-sulfur batteries," *Angew. Chem., Intl. Ed.* 50(26), 5904-5908. DOI:10.1002/anie.201100637
- Kang, B., and Ceder, G. (2009). "Battery materials for ultrafast charging and discharging," *Nature* 458(3), 190-193. DOI: 10.1038/nature07853
- Kicinski, W., Szala, M., and Bystrzejewski, M. (2014). "Sulfur-doped porous carbons: Synthesis and applications," *Carbon* 68(11), 1-32. DOI: 10.1016/j.carbon.2013.11.004
- Kolosnitsyn, V. S., and Karaseva, E. V. (2008). "Lithium-sulfur batteries: Problems and solutions," *Russ. J. Electrochem* 44(5), 506-509. DOI:10.1134/S1023193508050029
- Kruk, M., and Jaroniec, M. (2002). "Determination of mesopore size distributions from argon adsorption data at 77 K," *J. Phys. Chem. B* 106(18), 4732-4739. DOI: 10.1021/jp0137423
- Kumaresan, K., Mikhaylik, Y., and White, R. E. (2008). "A mathematical model for a lithium-sulfur cell," *J. Electrochem. Soc.* 155(8), 576-582. DOI:10.1149/1.2937304
- Lee, K. T., Black, R., Yim, T., Ji, X., and Nazar, L. F. (2012). "Surface-initiated growth of thin oxide coatings for Li-sulfur battery cathodes," *Adv. Energy. Mater.* 2(12), 1490-1496. DOI: 10.1002/aenm.201200006
- Li, X., Cao, Y., Qi, W., Saraf, L. V., Xiao, J., Nie, Z., *et al.* (2011). "Optimization of mesoporous carbon structures for lithium-sulfur battery applications," *J. Mater. Chem.* 21(41), 16603-16610. DOI: 10.1039/C1JM12979A
- Liang, C., Dudney, N. J., and Howe, J. Y. (2009). "Hierarchically structured sulfur/carbon nanocomposite material for high-energy lithium battery," *Chem. Mater* 21(19), 4724-4730. DOI: 10.1021/cm902050j
- Manthiram, A., Murugan, A. V., Sarkar, A., and Muraliganth, T. (2008). "Nanostructured electrode materials for electrochemical energy storage and conversion," *Energy Environ. Sci.* 1(6), 621-638. DOI:10.1039/B811802G
- Mikhaylik, Y. V., and Akridge, J. R. (2004). "Polysulfide shuttle study in the Li/S battery system," *J. Electrochem. Soc.* 151(11), 1969-1976. DOI:10.1149/1.1806394
- Moreno, N., Caballero, A., Hernan, L., and Morales, J. (2014). "Lithium-sulfur batteries with activated carbons derived from olive stones," *Carbon* 70(3), 241-248. DOI:10.1016/j.carbon.2014.01.002
- Peled, E., Eshkenazi, V., and Rosenberg, Y. (1998). "Study of lithium insertion in hard carbon made from cotton wool," *J. Power Sources* 76(2), 153-158. DOI: 10.1016/S0378-7753(98)00148-7
- Park, M. S., Yu, J. S., Kim, K. J., Jeong, G., Kim, J. H., Yim, T., *et al.* (2013). "Porous carbon sphere as a functional conducting framework for use in lithium-sulfur batteries," *RSC Adv.* 3(29), 11774-11781. DOI: 10.1039/C3RA41061G
- Song, M. K., Cairns, E. J., and Zhang, Y. (2013). "Lithium/sulfur batteries with high specific energy: Old challenges and new opportunities," *Nanoscale* 5(6), 2186-2204. DOI: 10.1039/C2NR33044J

- Scrosati, B., Hassoun, J., and Sun, Y. K. (2011). "Lithium-ion batteries. A look into the future," *Energy Environ. Sci.* 4(9), 3287-3295. DOI: 10.1039/C1EE01388B
- Shim, J., Striebel, K. A., and Cairns, E. J. (2002). "The lithium/sulfur rechargeable cell: Effects of electrode composition and solvent on cell performance," *J. Electrochem. Soc.* 149(10), 1321-1325. DOI:10.1149/1.1503076
- Sun, X. G., Wang, X. Q., Mayes, R. T., and Dai, S. (2012). "Lithium—sulfur batteries based on nitrogen-doped carbon and an ionic-liquid electrolyte," *Chem Sus Chem* 5(10), 2079-2085. DOI: 10.1002/cssc.201200101
- Tarascon, J. M., and Amand, M. (2001). "Issues and challenges facing rechargeable lithium batteries," *Nature* 414(11), 359-367. DOI:10.1016/j.materresbull.2007.08.031
- Thackeray, M. M., Wolverton, C., and Isaacs, E. D. (2012). "Electrical energy storage for transportation—Approaching the limits of, and going beyond lithium-ion batteries," *Energy Environ. Sci.* 5(7), 7854-7863. DOI: 10.1039/C2EE21892E
- Wang, J., Chew, S. Y., Zhao, Z. W., Ashraf, S., Wexler, D., Chen, J., Ng, S., Chou, S. L., and Liu, H. K. (2008). "Sulfur-mesoporous carbon composites in conjunction with a novel ionic liquid electrolyte for lithium rechargeable batteries," *Carbon* 46(2), 229-235. DOI:10.1016/j.carbon.2007.11.007
- Wang, C., Chen, J., Shi, Y., Zheng, M., and Dong, Q. (2010). "Preparation and performance of a core-shell carbon/sulfur material for lithium/sulfur battery," *Electrochim. Acta* 55(23), 7010-7015. DOI: 10.1016/j.electacta.2010.06.019
- Wang, H., Yang, Y., Liang, Y., Robinson, J. T., Li, Y., Jackson, A., Cui, Y., and Dai, H. (2011). "Graphene-wrapped sulfur particles as a rechargeable lithium-sulfur battery cathode material with high capacity and cycling stability," *Nano Lett.* 11(7), 2644-2647. DOI: 10.1021/nl200658a
- Wang, H., Yang, Y., Liang, Y., Cui, L., Casalongue, H. S., Li, Y., Hong, G., Cui, Y., and Dai, H. (2011). "LiMn_{1-x}FexPO₄ nanorods grown on graphene sheets for ultrahigh-rate-performance lithium ion batteries," *Angew. Chem., Intl. Ed.* 50(31), 7364-7368. DOI: 10.1002/anie.201103163
- Wei, L., Nitta, N., and Yushin, G. (2013). "Lithographically patterned thin activated carbon films as a new technology platform for on-chip devices," *ACS Nano* 7(8), 6498-6506. DOI: 10.1021/nl4028129
- Wei, L., Sevilla, M., Fuertes, A. B., Mokaya, R., and Yushin, G. (2012). "Polypyrrole-derived activated carbons for high-performance electrical double-layer capacitors with ionic liquid electrolyte," *Adv. Funct. Mater.* 22(4), 827-834. DOI: 10.1002/adfm.201101866
- Yang, Y., Zheng, G., and Cui, Y. (2013). "Nanostructured sulfur cathodes," *Chem. Soc. Rev* 42(7), 3018-3032. DOI: 10.1002/chin.201324187
- Yan, J., Wei, T., Shao, B., Fan, Z., Qian, W., Zhang, M., and Wei, F. (2009). "Preparation of a graphene nanosheet/polyaniline composite with high specific capacitance," *Carbon* 48(2), 487-493. DOI: 10.1016/j.carbon.2009.09.066
- Yin, L., Wang, J., Yang, J., and Nuli, Y. (2011). "A novel pyrolyzed polyacrylonitrile-sulfur@MWCNT composite cathode material for high-rate rechargeable lithium/sulfur batteries," *J. Mater. Chem.* 21(19), 6807-6810. DOI: 10.1039/C1JM00047K
- Zhang, W., Qiao, D., Pan, J., Cao, Y., Yang, H., and Ai, X. (2013). "A Li⁺-conductive microporous carbon-sulfur composite for Li-S batteries," *Electrochim. Acta* 87(9), 497-502. DOI: 10.1016/j.electacta.2012.09.086

- Zhang, J., Xiang, J., Dong, Z., Liu, Y., Wu, Y., and Xu, C. (2014). "Biomass derived activated carbon with 3D connected architecture for rechargeable lithium-sulfur batteries," *Electrochim. Acta* 116(11), 146-151. DOI: 10.1016/j.electacta.2013.11.035
- Zheng, G., Yang, Y., Cha, J. J., Hong, S. S., and Cui, Y. (2011). "Hollow carbon nanofiber-encapsulated sulfur cathodes for high specific capacity rechargeable lithium batteries," *Nano Lett.* 11(10), 4462-4467. DOI: 10.1021/nl2027684
- Zheng, W., Liu, Y., Hu, X., and Zhang, C. (2006). "Novel nanosized adsorbing sulfur composite cathode materials for the advanced secondary lithium batteries," *Electrochim. Acta* 51(7), 1330-1335. DOI: 10.1016/j.electacta.2005.06.021
- Zhou, G., Pei, S., Li, L., Wang, D-W., Wang, S., Huang, K., Yin, L. C., Li, F., and Cheng, H. M. (2014). "A graphene-pure-sulfur sandwich structure for ultrafast, long-life lithium-sulfur batteries," *Adv. Mater* 26(4), 625-631. DOI: 10.1002/adma.201302877

Article submitted: September 15, 2014; Peer review completed: October 25, 2014;

Revised version accepted: November 1, 2014; Published: November 11, 2014.